Journal of Materials Chemistry B

# Facile Fabrication of Polydopamine Nanotubes for Combined Chemo-Photothermal Therapy

| | |
|---|---|
| Journal: | *Journal of Materials Chemistry B* |
| Manuscript ID | TB-ART-07-2019-001338.R1 |
| Article Type: | Paper |
| Date Submitted by the Author: | 05-Sep-2019 |
| Complete List of Authors: | Sun, Yuzhe; Auburn University, Materials Research and Education Center<br>Davis, Edward; Auburn University, Materials Research and Education Center |
| | |

ARTICLE

# Facile Fabrication of Polydopamine Nanotubes for Combined Chemo-Photothermal Therapy

Received 00th January 20xx,
Accepted 00th January 20xx

DOI: 10.1039/x0xx00000x

Yuzhe Sun[a] and Edward W. Davis*[a]

We report a novel synthesis scheme to produce polydopamine (PDA) nanotubes using halloysite clay nanotubes (HNT) as a sacrificial template. Polydopamine nanotubes were fabricated via the formation of a polydopamine coating from a dopamine solution on HNT followed by template removal. Michael Addition was used to decorate the outer surface with polyethylene glycol. Removal of the template material resulted in a bilayered organic nanotube consisting of an inner layer of polydopamine adjacent to the lumen and an outer polyethylene glycol surface. The tubes had an aspect ratio of 5.3 ± 0.6, a diameter on the order of 70 nm, and wall thicknesses on the order of 15 nm. The PDA nanotubes exhibited photothermal conversion upon irradiation at near infrared wavelengths; a temperature increase of 30 °C was observed when a 250 μg/ml sample was subjected to 1 W cm-2 density irradiation at 808 nm wavelength. Analysis indicated that the prepared tubes had slightly higher photothermal conversion efficiency than PDA nanospheres. An antitumor drug, doxorubicin, was used as a model to test the potential for drug delivery of the organic nanotubes. The nanotubes exhibited higher loading capacities than PDA nanospheres and were capable of controlled release at pHs relevant to human serum and tumors (pH 7.4 and 5.0 respectively). Drug release rates varied as a function of system pH and application of near infrared irradiation. Release of doxorubicin was enhanced at pH of 5.0, and retarded at a pH of 7.4. Irradiation with 808 nm wavelength light also increased the release of doxorubicin.

## Introduction

Polydopamine (PDA), a promising material for biomedical applications, was first explored by Messersmith's group in 2007.[1] The highly active catechol and amino groups in dopamine allow for polymerization under mild base conditions.[2, 3] In addition, the facile attachment to surfaces has been used for the functionalization of many nanoparticle systems including $Fe_3O_4$, noble metals, and others.[4-10] Functional groups with amino/thiol ends can also be attached to PDA via Michael addition and/or Schiff base reaction under similar mild base conditions.[11] Mild reaction conditions and facile surface modification has motivated the exploration of PDA nanoparticles in a range of applications.[12, 13] PDA has low hemolytic activity and no acute toxicity has been noted in either *in vitro* or *in vivo* tests, indicating that it has excellent biocompatibility.[2] A comprehensive study on PDA biodegradability has not been conducted. However, it is chemically similar to melanin, a natural pigment found in a wide variety of plants, animals, and microorganisms. In animals, melanin is degraded in phagosomes within phagocytic cells of the immune system.[14-18] These vesicles contain nicotinamide adenine dinucleotide phosphate (NADPH) oxidase which has been shown to produce reactive oxygen species (ROS). Several groups have demonstrated the degradation of both melanin and PDA in the presence of ROS suggesting that PDA should undergo biodegradation similar to melanin.[2, 19-21] The plentiful amino and catechol groups enable PDA to reversibly bind to other compounds via intermolecular interactions such as hydrogen bonding and π-π interactions. The influence of pH on binding strength suggests the ability to utilize PDA nanoparticles as nanocarriers for controlled delivery to tumours.[22-24] PDA also exhibits significant absorbance at infrared wavelengths suggesting it may have applications in photothermal therapies[2, 25-28] and as a combined chemo-photothermal agent.[4, 29-35] Several studies highlight the morphology dependent behaviour of polydopamine.[36-38] These studies, particularly those demonstrating shape dependent photothermal and drug loading behaviour, suggest that novel shapes of PDA nanotubes may exhibit enhanced performance over the traditional spherical particle.

Extensive studies have been conducted exploring the effect of nanoparticles size, surface chemistry, and composition on cellular uptake and drug delivery.[39-42] Recent studies indicate that particle shape also plays a key role in controlling cellular uptake, with rods exhibiting reduced uptake by circulating phagocyctes, leading to prolonged circulation time as compared to spherical particles.[43-49] In addition to the prolonged circulation exhibited by nanorods, studies have demonstrated that high aspect ratio rods exhibit greater tumour accumulation and deeper tumour penetration.[50, 51] In vitro investigations have demonstrated low non-specific[43, 52-54] and high-specific[55-57] cellular uptake of nanorods. While the interaction between nanoparticle shape and physiological environment is not

[a] *Materials Engineering Program, Auburn University, 274 Wilmore Labs, Auburn Alabama, United States.*

completely understood and there are some studies implying the potential negative influence of rod-like shape on biocompatibility,[58-60] nanoparticle shape undoubtfully plays a role in biodistribution and cellular uptake. This dependence suggests enhanced performance of anisotropic materials in targeted drug delivery.

Several methods have been developed for producing non-spherical micro/nanostructures including microfluidics,[45, 61-63] projection photolithography,[45, 64] particle replication in non-wetting templates (PRINT),[65] film-stretching,[66] self-assembly,[67-71] and template-assisted fabrication.[72] Despite the advance in shape control of micro/nanostructures, there remain significant limitations in the application of these techniques to cancer therapy. For example, to avoid clearance by the MPS, liver, spleen, and kidney; and to capitalize on the enhanced permeability and retention of these particles by tumour cells, the optimal nanoparticle sizes are believed to be in the range of 30-200 nm.[73] Methods such as microfluidics, projection photolithography, PRINT method, and templating with porous anodic aluminium oxide produce nanoparticles outside this desired size range.[45, 65, 74-76] In addition these methods carry relatively high synthesis costs. [77] Film-stretching is a versatile technique capable of producing several geometries of polymeric nanoparticles. However, the nanoparticles obtained through film-stretching are all solid, limiting the ability to load therapeutic agents.[44] Self-assembly techniques utilize the formation of micelle and vesical shaped nanostructures in a liquid colloid, and are capable of producing particles in the requisite size range. However, the specific shape and size dispersity can be difficult to control.[45] Particles derived from self-assembly, can be used as soft templates for synthesis of polymeric nanotubes as can other hard templates.[78, 79] Carbon nanotubes can be surface modified with a wide variety of organic materials using both physical adsorption and chemical grafting.[80-82] However, the CNTs remain in the obtained nanoparticles. In template-assisted methods, the shape, size and polydispersity of fabricated nanostructures are largely dependent on the template utilized. These methods have been used to produce nanomaterials with various shapes, such as nanocubes, nanoellipsoids, and nanopeanuts.[83] Recently PDA nanorods have been fabricated via the use of rod-like templates such as curcumin crystals and ZnO nanorods.[84-86] However, the rods obtained are larger than the 30-200 nm range desired to avoid clearance and enhance accumulation at tumour sites. Thus, while shape is potentially a powerful factor to enhance cancer treatment the formation of high aspect ratio polymeric nanoparticles, particularly polymeric nanotubes, in the appropriate size range is not a simple task.

Naturally occurring silicate nanotubes, most notably halloysite, have been used as a template for inorganic nanostructures such as nanorods, formed in the inner pore, and there are numerous reports of grafting polymers to their surfaces.[87-89] Halloysite nanotubes (HNTs) are formed by the rolling of kaolinite resulting in a hollow lumen with a diameter of 12-15 nm and an overall diameter of 50-60 nm.[90, 91] The tubular structure, low cost, and biologically inertness of halloysite has driven its development as a controlled release reservoir.[92-94] Unfortunately, HNTs are not biodegradable and are not removed from the circulatory system via the kidneys limiting suitability for direct drug delivery.[95] More recently halloysite has been used to produce polymer coated nanotubes via surface copolymerization of propyl methacrylate, ethylene glycol dimethacrylate, and methacrylic acid, and by the deposition of polypyrrole from HCl solution.[96, 97]

This work leverages the simplicity of preparing conformal coatings of PDA and the availability of the low cost natural nanotube halloysite for the facile preparation of high aspect organic nanotubes that combine the benefits of PDA with the increased circulation time and tumour uptake reported for nanorods. Residual catechol and amino groups were used to further modify the PDA surface. The pH and photothermal behaviour of the particles can be used to control release rates of therapeutic compounds loaded either during or after fabrication. The morphology and photothermal behaviour of the resulting PEG coated PDA nanotubes as well as the loading and release characteristics of a model chemotherapeutic compound, doxorubicin (DOX), from these nanotubes are reported. Results are compared with PDA nanospheres. The resulting PDA nanotubes have potential application as combined photothermal / drug delivery systems.

## Results and discussion

### Fabrication of Polydopamine based Nanostructures

Scheme 1 depicts the nanotube fabrication process. Dopamine undergoes a self-oxidation process in weak base conditions.[1] Through a series of oxidation, cyclization and isomerization reactions, dopamine molecules conjugate and form a conformal polydopamine coating on the suspended particles.[19] By suspending HNTs in a dopamine solution in Tris buffer a conformal coating on the halloysite surface was formed as the reaction proceeded. In this work, halloysite was suspended first followed by the addition of dopamine under rapid stirring. After addition of dopamine, the color of the medium quickly changed to pink, indicating oxidation of the catechol groups and formation of indoles. The solution gradually turned dark brown as polymerization proceeded. Fig. 1(a) and (b) are TEM images of unmodified HNTs, and PDA coated halloysite, PDA-HNT. As compared to the unmodified halloysite the coated halloysite had a larger diameter and a rougher surface. Further modification of the nanotube was achieved by addition of amine terminated PEG ($M_w$ – 1000). Reaction between the amine terminal group and quinone groups on the PDA coating effectively grafted PEG to the tube surface. Fig. 1(c) is an TEM image of PEG grafted PDA coated halloysite nanotubes, PEG-PDA-HNT. In general, the tubes had a similar diameter to PDA-HNT with a similar surface roughness. Removal of the halloysite was achieved by HF etching. Fig. 1(d) is a TEM image of the resulting PEG-PDA bilayer nanotubes (PEG-PDA-NT). The tubes had considerably lower stiffness than halloysite, as evidenced by the appearance of bent, wrinkled, flattened, or otherwise distorted, nanotubes. HNTs have both an outer and inner surface available for PDA deposition. Based on TEM images,

only a single layer of PDA was left after HF etching of PDA coated HNTs. Thus, either there was no PDA deposited on the inner surface of halloysite, possibly due to diffusion limitations, or the PDA deposited on the inner surface of halloysite is removed

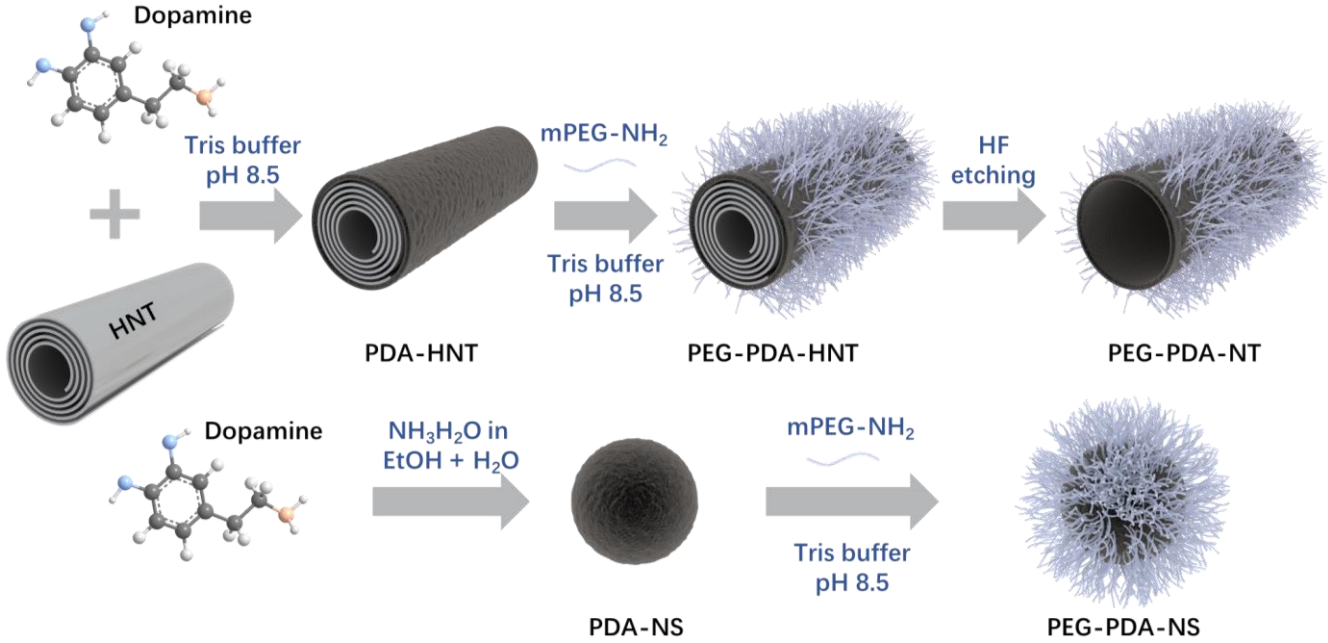


**Scheme 1** Synthesis of polyethylene glycol coated polydopamine bilayer tubes begins with the formation of a conformal coating of polydopamine on halloysite nanotubes. Surface modification of the polydopamine is achieved through reaction with amine terminated polyethylene glycol. The halloysite template is then removed by etching with hydrofluoric acid. Synthesis of polyethylene glycol coated polydopamine spheres begins with the production of polydopamine spheres from a dopamine solution followed by reaction with amine terminated polyethylene glycol.

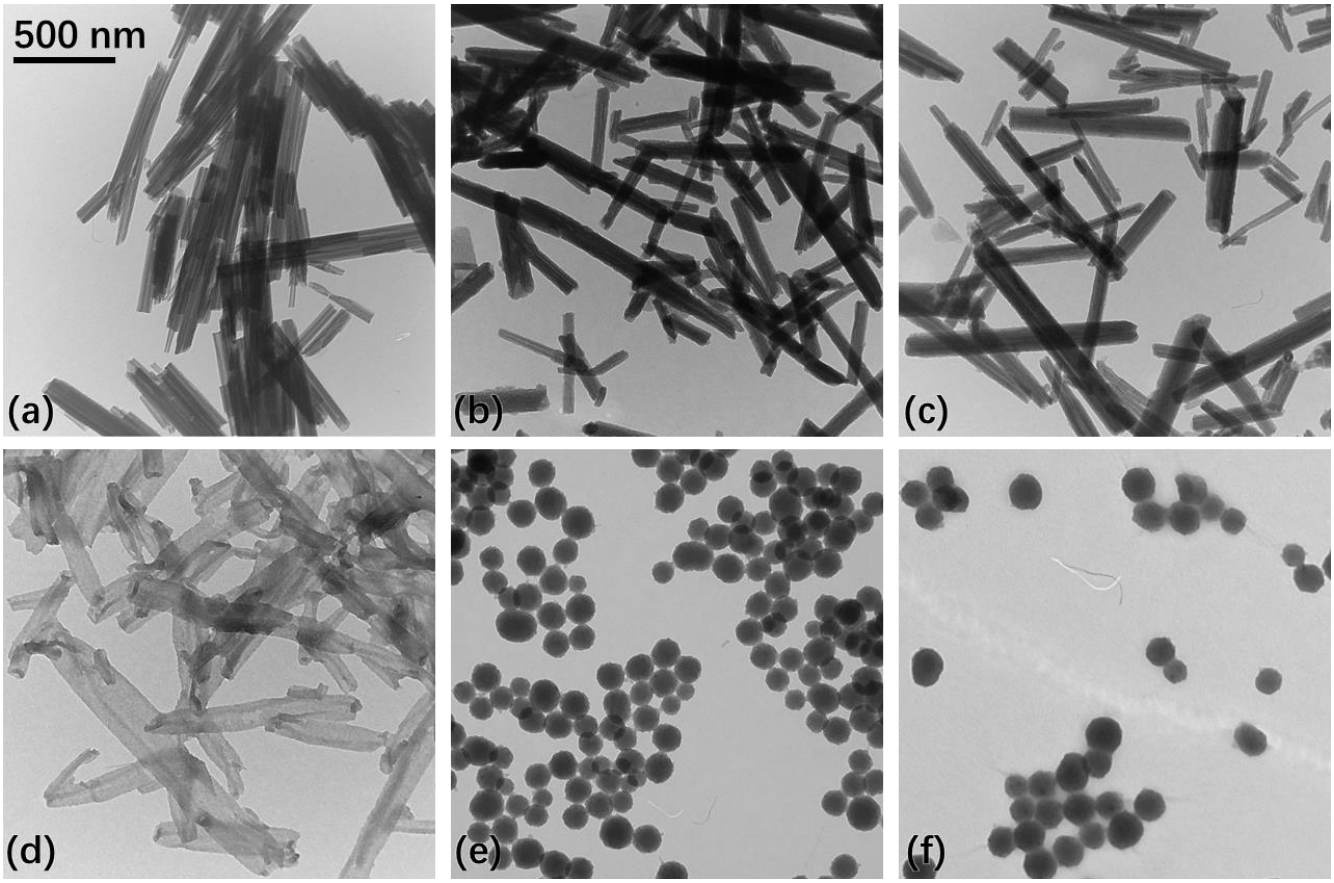


**Fig. 1** TEM images of nanotubes and nanospheres: (a) unmodified halloysite, (b) polydopamine coated halloysite, (c)polyethylene glycol surface modified polydopamine coated halloysite, (d)polyethylene glycol surface modified polydopamine nanotubes, (e) polydopamine nanospheres, and (f)polyethylene glycol surface modified polydopamine nanospheres.

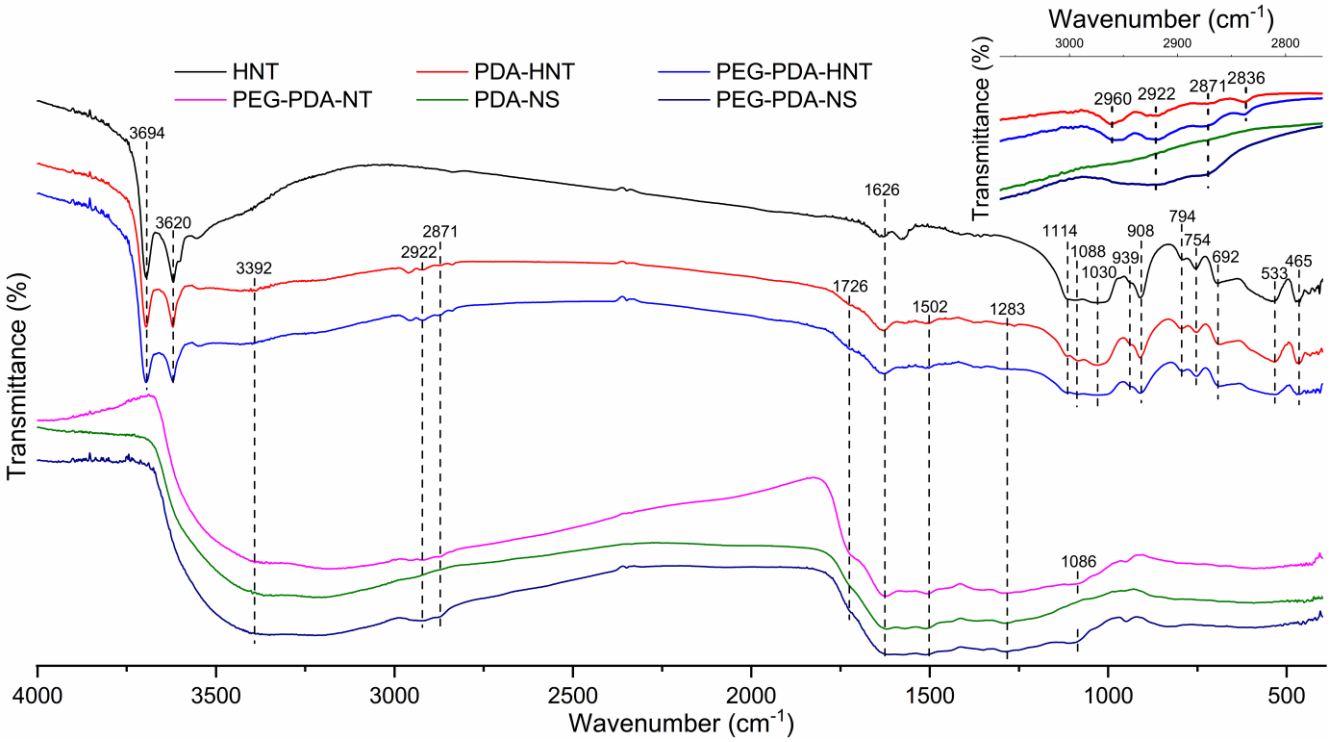


**Fig. 2** FTIR spectra of halloysite and nanomaterials produced in this work.

with the HNT upon etching. The diameter of pristine HNT was 51-60 nm, the diameter of PDA coated HNTs was ~25% larger, 65-75 nm. PEG modification resulted in a small additional increase in diameter, 67-78 nm. After HF etching, possibly due to partial collapse of nanotubes into less cylindrical shapes, the width measured under TEM was 104-127 nm small enough for transport through the leaky vessel walls typical of tumours (< 200 nm) and large enough to avoid clearance by the kidneys (>10 nm).[73] Lengths obtained for the tubes ranged were 532 – 709 nm; the aspect ratios were in the range of 4.7 to 5.9. For comparison PDA spheres, PDA-NS, and PEG coated PDA spheres, PEG-PDA-NS, were produced by the method reported by Liu et al.[2] Solid spheres were selected as a comparison as they are the most studied form of PDA nanoparticles. In addition, the inner surface of hollow spheres is not directly accessible. In contrast the inner surface of an open tube such as those produced in this work is accessible via the tube ends. The PDA spheres produced, Fig. 1(e) and (f), had diameters of ~115-130 nm and 145–160 nm respectively. The comparatively thin PDA layers in the prepared nanotubes versus the size of the PDA nanospheres is explained by the modulation of PDA growth in Tris buffer as seen in the work of Della Vecchia et al.[98] Under TEM, the hollow nanotubes were semi-transparent, most notably for the PEG-PDA-NT, while the solid nanospheres were opaque.

Representative FTIR spectra, Fig. 2, show typical peaks for HNT in not only the pristine halloysite, but also the PDA-HNT and PEG-PDA-HNT tubes. These peaks include the O-H stretching of hydroxyl groups at 3694 and 3620 $cm^{-1}$, as well as the deformation and stretching of Si-O, Al-O-Si, and OH in the range of 465-1114 $cm^{-1}$, consistent with previous studies.[87] However, after HF etching, these peaks disappeared, indicating complete removal of template. Compared with pristine halloysite, a wide arch was present in the spectra from about 1850 to 3650 $cm^{-1}$ after the PDA coating was formed.[77, 99] This arch was more obvious after HNT etching. The peaks at 1283 $cm^{-1}$ and 1502 $cm^{-1}$ correspond to the stretching vibrations of C-N, C=C, and C=NC of aromatic rings, while the peak at 1726 $cm^{-1}$ corresponds to the stretching vibration of C=O, all indicate the presence of PDA.[77, 100] After PEG modification, small peaks appeared at 2922 $cm^{-1}$ and 2871 $cm^{-1}$. These are attributed to the asymmetric and symmetric stretching vibrations of -$CH_2$ in PEG.[77, 99, 101] The peak at 1086 $cm^{-1}$, attributed to the stretching vibration of $CH_2$-C-O, also suggests the PEGylation of PDA. There were also two peaks at 2836 and 2960 $cm^{-1}$ found on PDA-HNT and PEG-PDA-HNT which disappeared after HF etching. The authors believe these peaks are associated with aliphatic C-H groups interacting with the halloysite surfaces. This interaction disappears after halloysite removal. Similar features are noted in the spectra of PDA-NS and PEG-PDA-NS.

Thermogravimetric analysis (TGA) was performed to study the composition of nanotubes, Fig. 3. To eliminate interference of moisture with the analysis, the sample weight at 100 ℃ was selected to be representative of samples without adsorbed water. For the unmodified HNT, around 15.4 % of the sample mass was lost between 450 and 550 °C, peak loss occurred at 508 °C, Fig. 3(b). This peak is typically assigned to the dehydroxylation of structural Al-OH groups of HNT.[101, 102] Conversely polydopamine coated halloysite exhibited mass loss between 200 and 600 ℃. Pure PDA exhibits a mass loss across a broad temperature range in TGA testing supporting the assignment of this loss peak to the presence of PDA.[103] In total 37.2% of the mass was lost for PDA-HNTs. Two events were responsible for this behaviour, Fig. 3(b). The first, related to PDA

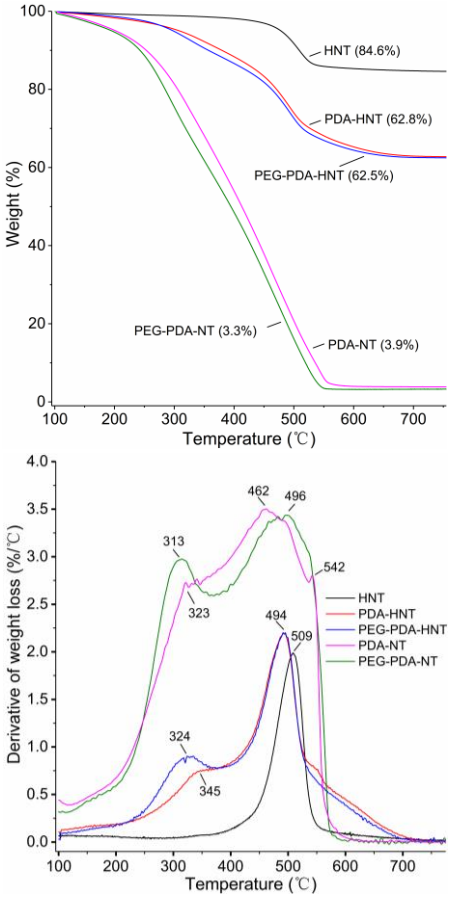


**Fig. 3** (a) TGA curves for nanotubes. Numbers in parenthesis refer to residual mass at end of test. (b) Derivative of weight loss versus temperature measured by TGA of nanotubes.

degradation, was centred at 345 °C and the second, related to dihydroxylation of HNT, was centred at 494 °C. Analysis indicates that dehydroxylation accounted for 30.2% of the lost mass while PDA degradation accounted for 69.8%. This suggest that the PDA-HNT tubes are roughly 26 wt.% PDA. Similar results were obtained after modification with polyethylene glycol; dehydroxylation accounted for 29.8% of the total weight lost while the combined PDA and PEG degradation accounted for 70.2% of the total weight lost. The total loss was 37.5% suggesting the PEG-PDA-HNT tubes are 26.3 wt.%. After etching of the halloysite the dehydroxylation peak largely disappears and almost the entire mass of the sample is degraded during TGA testing, 3.9% residual mass for polydopamine nanotubes and 3.3% residual mass for polyethylene glycol coated polydopamine nanotubes indicating the halloysite template was completely removed. This result is consistent with the TEM and FTIR analysis.

**Drug Loading Capacity**

Loading of doxorubicin was accomplished by adsorption from a concentrated solution. In the aqueous solution used to load the nanoparticles, 10 mM PBS at pH 8, doxorubicin is positively charged while PDA is negatively charged resulting in a strong driving force for the adsorption of doxorubicin by PDA.[22, 104, 105] Doxorubicin also interacts with PDA through π - π and hydrogen bonding interactions increasing binding and loading capacity.[29] In this work, solutions with various doxorubicin concentrations, 0.1 mg/ml to 1.5 mg/ml, were used to load the nanoparticles. Two methods were used to evaluate the amount of doxorubicin loaded on the nanoparticles. First, after loading, the collected and washed nanoparticles were resuspended in Tris buffer and UV-Vis spectra taken. PDA exhibits a wide absorbance from 300 to 800 nm. However, adsorbed doxorubicin increases the adsorption particularly between 450 and 550 nm. Fig. 4(a) shows spectra obtained from doxorubicin loaded PEG-PDA-NT, which was washed and resuspended after loading. As the concentration of doxorubicin in the loading solution increased, the absorbance between 450 and 550 nm increased, suggesting a higher loading was achieved; dispersions with the same concentration of PEG-PDA-NT were used in each case. Due to the significant spectral overlap between PDA and doxorubicin, comparison of the UV-Vis absorption of loaded nanoparticle dispersions is qualitative.

Quantification of doxorubicin loading was obtained by an indirect calculation. In this case, the residual doxorubicin concentration in the supernatant remaining after collection and washing of the loaded nanoparticles was used to determine the

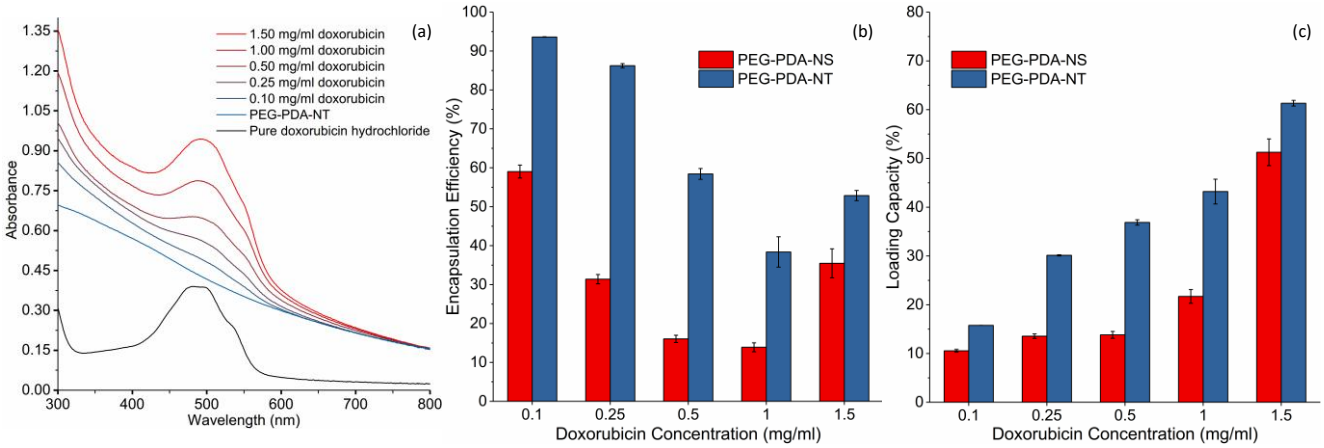


**Fig. 4** Characterization of doxorubicin loading on polydopamine nanoparticles. (a) UV/Vis spectra of PEG-PDA-NT/Dox loaded with different doxorubicin concentrations, pure PEG-PDA-NT, and doxorubicin hydrochloride. (b) Encapsulation efficiency of doxorubicin on PDA nanoparticles. (c) The loading capacity of doxorubicin on PDA nanoparticles. Error bars in (c) and (d) are standard error.

amount of doxorubicin not loaded on the nanoparticles. The encapsulation efficiency (EE) was calculated from:

$$\mathrm{EE} = \frac{\mathrm{c_{LS}} \cdot \mathrm{V_{LS}} - \mathrm{c_S} \cdot \mathrm{V_S}}{\mathrm{c_{LS}} \cdot \mathrm{V_{LS}}} \times 100\%$$

where EE is fraction of doxorubicin that was loaded onto the nanoparticles, $c_{LS}$ is the doxorubicin concentration in the loading solution, $V_{LS}$ is the volume of loading solution used, $c_S$ is the doxorubicin concentration in the supernatant collected during washing, and $V_S$ is the volume of supernatant collected during washing. As shown in Fig. 4(b), as the doxorubicin concentration in the loading solution increased, the encapsulation efficiency dropped from 95% (0.1 mg/ml doxorubicin solution) to 37% (1 mg/ml doxorubicin solution). This trend was interrupted when the concentration was increased to 1.5 mg/ml, the encapsulation efficiency for PEG-PDA-NT increased to 55% at this concentration. Similar trends in the loading efficiency for PEG-PDA-NS were observed. However, at every concentration, the encapsulation efficiency for PEG-PDA-NT was higher than that for PEG-PDA-NS, this can be attributed to the higher specific area of nanotubes. The enhanced efficiency at the highest loading concentration is believed to result from diffusion of the adsorption of doxorubicin into bulk PDA. If bulk absorption plays a role in encapsulation efficiency, one would expect that it is the total mass of PDA that would control loading efficiency, and there would be no significant difference between nanospheres and nanotubes. When loading solution concentrations were between 0.1 and 1.0 mg/ml, the encapsulation efficiency of PEG-PDA-NS was roughly 60% of the PEG-PDA-NT. However, when a loading solution of 1.5 mg/ml was used, the ratio increased to ~85% supporting the hypothesis that loading shifts from a surface to a bulk effect. This effect is similar that observed by Zeng et. al. for the diffusion of $Au^{3+}$ into a PDA shell.[10]

The loading capacity (LC) was calculated from:

$$\mathrm{LC} = \frac{\mathrm{c_{LS}} \cdot \mathrm{V_{LS}} - \mathrm{c_S} \cdot \mathrm{V_S}}{\mathrm{M_{NP}} + \mathrm{c_{LS}} \cdot \mathrm{V_{LS}} - \mathrm{c_S} \cdot \mathrm{V_S}} \times 100\%$$

where, LC is the fraction of the mass of loaded doxorubicin divided by the total mass of the nanoparticles after loading, and $M_{NP}$ is the mass of the unloaded nanoparticles. Loading capacity of doxorubicin on nanoparticles is shown in Fig. 4(c). Loading capacity increased as doxorubicin concentration increased in the loading solution. For PEG-PDA-NT, the doxorubicin fraction increased from ~15.8% to ~61.3% as the loading solution doxorubicin concentration increased from 0.1 to 1.5 mg/ml. Loading with mass fractions greater than 50%, while surprising, are not unheard of for particles with large specific surface area.[106] Similar trends were noted for PEG-PDA-NS. The loading capacity of the nanospheres is lower than that of the nanotubes at all concentrations. However, the relative loading capacity, nanosphere loading capacity divided by nanotube loading capacity, does seem to be a function of doxorubicin concentration in the loading solution. When the doxorubicin concentration in the loading solution was 0.1 mg/ml, the relative loading capacity was 67%. It dropped to 34% when the doxorubicin concentration in the loading medium was 0.5 mg/ml and increased to 84% at a doxorubicin concentration in the loading medium of 1.5 mg/ml. This behaviour supports the idea that loading shifts from a surface to bulk driven phenomena at higher doxorubicin concentrations.

**Photothermal Behaviour**

Previously, Liu et al. demonstrated the high photothermal efficiency to PDA nanospheres, suggesting their applicability to photothermal therapy.[2] In this work the photothermal performance of PEG-PDA-NT were compared with PEG-PDA-NS prepared via Liu's method, Fig. 5. As expected, the heat up rate of NIR irradiated dispersions was largely dependent on mass concentration of PDA, Fig. 5(a) and (b). At high concentrations, 1 mg/ml, the dispersions displayed a 43 °C temperature rise over 15 minutes. While dispersions at concentrations of 50 μg/ml only exhibited an increase of ~10 °C. However, for both PEG-PDA-NT and PEG-PDA-NS the maximum temperature increase is not a linear function of concentration, Fig. 5(b), the apparent photothermal efficiency decreases. This decrease is possibly due to agglomeration of the nanoparticles.

The results in Fig. 5(a) suggest that PEG-PDA-NT have a higher photothermal efficiency that PEG-PDA-NS. For example at 250 μg/ml, the PEG-PDA-NS displayed a temperature change of 35.0 ℃, while the PEG-PDA-NT resulted in a 4.3 ℃ higher temperature change, 39.3 ℃, under the same conditions. Similar differences were apparent at all concentrations evaluated. To elucidate this difference the photothermal conversion efficiency, $\eta$, of both PDA nanoparticles were measured. Efficiency was calculated from:

$$\eta = \frac{hA\Delta T_{max} - Q_s}{I(1 - 10^{-A_\lambda})}$$

where $h$ is the heat transfer coefficient, $A$ is the surface area of the container, $\Delta T_{max}$ is the maximum temperature change of PDA nanoparticle dispersions at steady state, $I$ is the irradiation power, $A_\lambda$ is the absorbance 808 nm, and $Q_s$ is the heat associated with the light absorbance of the solvent.[2] $Q_s$ was calculated from $Q_s = hA\Delta T_{\mathrm{solvent}}$, where $\Delta T_{solvent}$ is the maximum temperature change of water irradiated by the same light source at the same power intensity. The parameter set $hA$ was determined by fitting temperature vs time data to the equation:

$$t = -\frac{\sum_i m_i c_{pi}}{hA} ln(\theta)$$

where, $m_i$ is the mass of component i, $C_{pi}$ is the specific heat capacity of component i, t is time, and $\theta$ is calculated at each time increment as $(\Delta T/\Delta T_{max})$. The summation $\sum_i m_i c_{pi}$ was approximated by the mass and specific heat capacity of the solvent (water). Data was collected as the photothermally heated sample cooled to room temperature, Fig. 5(c). The fits are shown in Fig. 5(f). The photothermal conversion efficiency of PEG-PDA-NS at 250 μg/ml was found to be 40%, the same value obtained by Liu et al.[2] The photothermal conversion

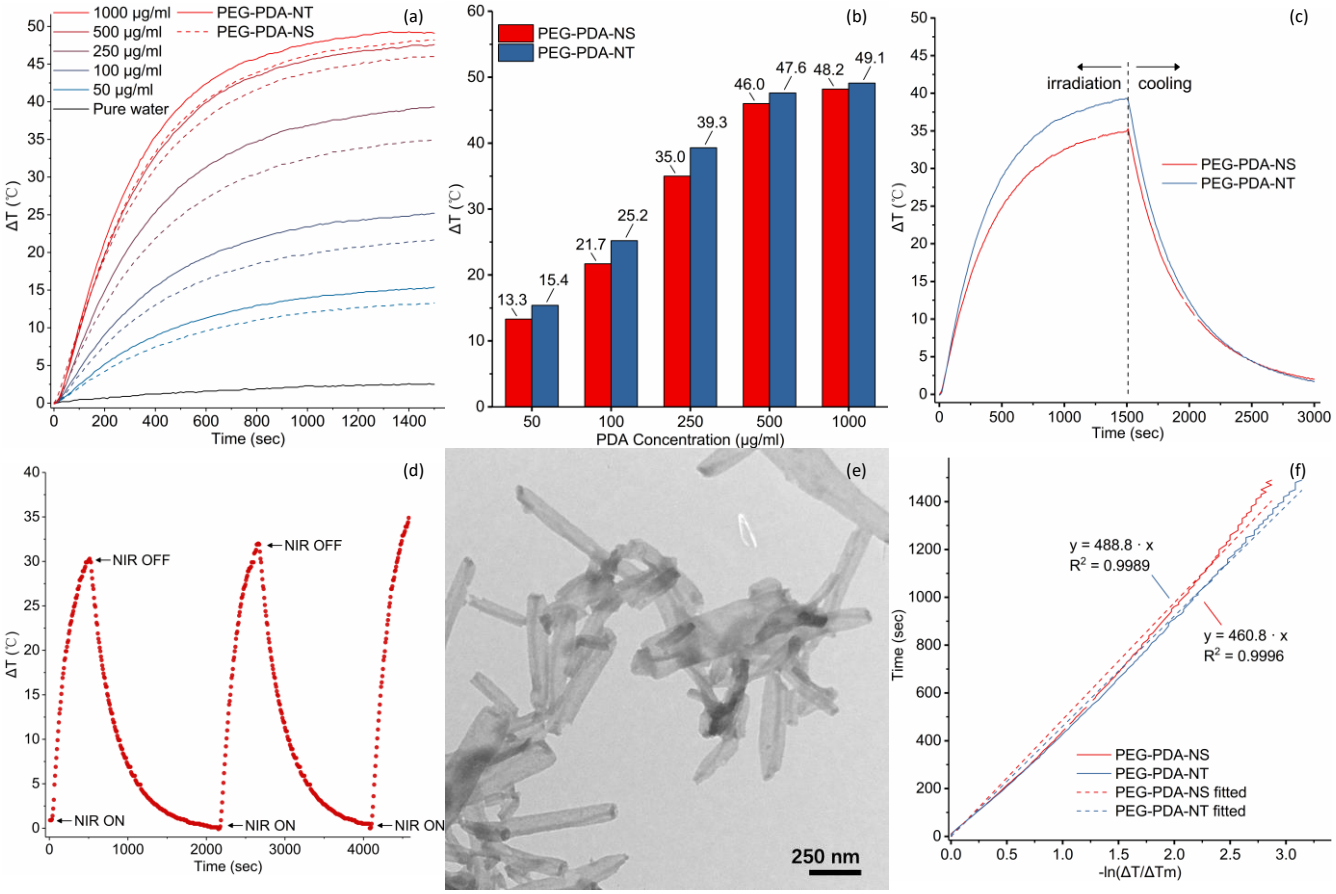


**Fig. 5** Photothermal behaviour of polyethylene glycol coated polydopamine nanotubes and nanospheres. (a) Temperature change over time of PEG-PDA-NT and PEG-PDA-NS dispersions in DI water upon irradiation by an 808 nm source at 1W/cm2 intensity. (b) Temperature change after irradiation, same conditions, for 1000 s for PEG-PDA-NT and PEG-PDA-NS dispersions as function of mass concentration. (c) Temperature change during irradiation and cooling period for 250 µg/ml PDA nanoparticles dispersion. (d) Cyclic photothermal behaviour of PEG-PDA-NT dispersion (1mg/ml). Sample irradiated for 500 seconds by an 808 nm sources at 1 W/cm2 followed by no irradiation until dispersion cooled to ambient temperature (~1500 s). (e) TEM of PEG-PDA-NT after cyclic irradiation. (f) Time versus −ln(ΔT/ΔTm) for cooling phase data shown in Fig. 6(c), used for determining hA values required to calculate photothermal efficiency.

efficiency for PEG-PDA-NT at the same mass concentration was found to be 42%.

Gold nanorods have been widely studied as a photothermal therapeutic agent, owing to localized surface plasmon resonance (LSPR).[107] However, according to Liu et al.'s study, gold nanorods experience significant morphology changes upon irradiation. One effect of this morphological change is a change in SPR resulting in a reduction of photothermal energy transfer.[2] In this study a dispersion of PEG-PDA-NT (1 mg/ml) was repeatedly irradiated at an energy density of 1 W $cm^{-2}$ with 808 nm wavelength light. The 1 mg/ml concentration of PEG-PDA-NT was selected to maximize the temperature change during the evaluation. The dispersion was irradiated for 500 seconds, followed by 1500 seconds cooling. This irradiation / cooling cycle was repeated several times on the same sample. The temperature of the dispersion was recorded over the course of the irradiation / cooling cycles, Fig. 5(d). It can be seen the photothermal effect of PEG-PDA-NT was not deteriorated by previous irradiations. The highest temperature of the dispersion even increased during the second and third irradiation. This increase is believed to be due to an increased PDA concentration due to water evaporation during the test. The morphology of PDA nanotubes after repeated NIR was inspected by TEM. As shown in Fig. 5(e), no obvious morphological changes were observed for the PEG-PDA-NT.

### Release Behaviour

Normally, the pH of blood is around 7.4, while in tumours, the pH drops to lower than 6.6; the pH of endosomes are in the range of 6.5 to 5.0.[108-110] Therefore, pH change is commonly used to trigger local release of therapeutic compounds. Under weak acidic conditions, such as those found in endosomes, the release rate of doxorubicin from the PDA nanoparticles produced in this work was faster and reached a higher level of completion. For tubes, after 24 h, ~55% of loaded doxorubicin was released when the media was at pH 5.0, while only ~17% doxorubicin was released in neutral pH. For spheres the fraction released at the same times was ~45% at pH 5.0, while only ~14% was released at neutral pH. The fraction of doxorubicin released from the tubes was ~20% higher than exhibited by the spheres at both pHs evaluated. The pH effect is similar to that reported by Wang et. al. for polydopamine-gadolinium-metallofullerene.[30] In that work differences in release rates were related to the change in zeta potential of the PDA nanoparticles, zeta potential of PDA is a strong function of pH. At pH 5.0 the zeta potential of the tubes and spheres was -19.6

mV and -20.3 mV respectively while at a pH of 7.4 the zeta potential of the tubes and spheres was -32.2 mV and -39.3 mV respectively. The increased difference in zeta potential did not have a significant effect on the difference in fraction of doxorubicin released in the present study. This suggests that the increase release rate for the PDA nanotubes is related to the increased surface area of tubes vs spheres. Furthermore, as the PDA nanotubes had a higher loading capacity, Fig. 6(b), the amount of doxorubicin released per unit mass of PDA in the nanoparticles was considerably higher for nanotubes than for nanospheres. Fig. 6(a) shows the mass of doxorubicin released per mass of PDA in the nanoparticles as a function of time and pH of the release medium for PDA nanoparticles loaded in a 0.5 mg/ml doxorubicin solution. Under this loading condition the PDA nanotubes had ~2.5 times the loading capacity of the PDA nanospheres. The mass of doxorubicin released for spheres is less than half of that delivered by the tubes at both high and low pH.

Fig. 6(b) shows the effect of NIR irradiation on the release of doxorubicin from PEG-PDA-NT. Samples were placed in a quartz cuvette and irradiated (808 nm, 1 W/cm$^2$) for 10 minutes every two hours. The mass of doxorubicin released was measured just before and just after each irradiation cycle. It can be seen that under both pH conditions NIR irradiation induced a burst of release. When the irradiation was removed, release rates seemed to slow or reverse. The overall doxorubicin release rate and the effect of NIR irradiation was higher for low pH media. The samples were immersed in a water bath to limit the temperature increase of the dispersion during irradiation. However, the strong NIR adsorption by PDA is not affected. This energy adsorption increases the particle temperature disrupting hydrogen and π-π bonding and shifting equilibrium toward unbound doxorubicin. The increased temperature also increases local diffusion rates increasing doxorubicin release. In this test, the release media was not refreshed; perfect sink conditions were not maintained. Thus, during the portion of the cycle without NIR irradiation the doxorubicin could be reabsorbed by the particles, resulting in an apparent decrease in the mass released seen for some samples.

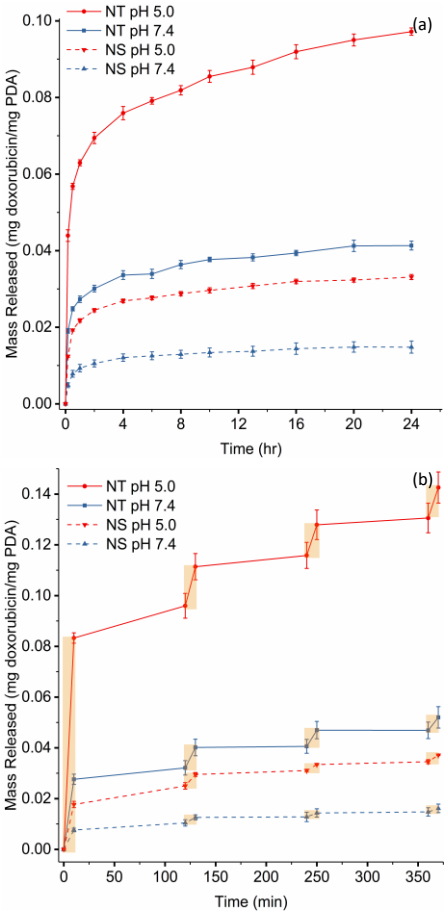


**Fig. 6** Release behavior of polydopamine nanotubes and nanospheres. (a) Mass of doxorubicin released per mass of PDA in the nanoparticles over time at two pHs. (b) Mass of doxorubicin released per mass of nanoparticles r over time when vessel is cyclically irradiated at 1W/cm2 by an 808 nm source. Highlighted rectangles indicate time sample is being irradiated. All error bars are standard error.

## Experimental

### Materials and instrumentation

Dopamine chloride (DA) was from Beantown Chemicals. Tris(hydroxymethyl) aminomethane (Tris) was obtained from VWR Life Science. Polyethylene glycol methyl ether amine (M.W. 1,000) (PEG-$NH_2$) was obtained from Alfa Aesar. Hydrochloric acid (HCl, 10 % v/v), potassium phosphate monobasic ($KH_2PO_4$), ammonia ($NH_3H_2$ in water, 28-30%), and potassium chloride (KCl) were obtained from BDH Chemicals. Sodium phosphate ($Na_2HPO_4$) and doxorubicin were obtained from MilliporeSigma. Sodium chloride (NaCl) was obtained from Fisher Scientific. Halloysite nanotubes (HNT) were obtained from Bonding Chemical. Hydrofluoric acid (50%, v/v ACS grade) was obtained from BDH Chemical. All chemicals were used without further purification. Deionized (DI) water was used in all the experiments. Morphology was obtained using transmission electron microscopy (TEM; Zeiss EM10). Samples were prepared by evaporation of dispersions onto a 300 mesh formvar/carbon film from Electron Microscopy Sciences. Fourier transform infrared spectra (FTIR) were obtained via a Shimadzu IR Prestige-21 FTIR spectrometer. KBr pellets were prepared at a sample to KBr ratio of 1:100. UV-Vis spectra were obtained on an Agilent Cary 60 UV-Vis, doxorubicin concentration in solution was obtained by measuring absorbance at 480 nm. Thermogravimetric analysis (TGA) was conducted on a Thermal Analysis TGA Q500. For every test, around 10 mg powder sample was used. The sample was ramped to 100 ℃ with a rate of 20 ℃/min. and the sample held isothermally at 100 ℃ for 2 minutes. The sample was then heated to 800 ℃ with a rate of 10 ℃/min. Zeta potential was obtained via a Malvern Instruments ZetaSizer Nano ZS90. Samples were dispersed in 1mM phosphate buffer at pH 7.4 or 1mM acetate buffer at pH 5.0.

### Synthesis

**Synthesis of polydopamine nanotubes (PDA-NT) and polyethylene glycol coated PDA nanotubes (PEG-PDA-NT).** In the first step PDA-HNTs were obtained via deposition of PDA

from an aqueous dopamine solution. In a typical synthesis 20 mg HNT was added in 70 ml of 10 mM Tris-HCl buffer and dispersed ultrasonically for two minutes at 100 W (QSonica LLC, Q500). The dispersion was then continuously stirred as 20 mg DA was added. The dispersion color quickly changed to pink in ~5 min., and then to dark brown over about 30 min. After 24 h stirring, the medium was completely opaque. The product (PDA-HNTs) was obtained via centrifugation (21,964g) on a Heraeus Megafuge 8 centrifuge (Thermo Scientific). The product was washed and recollected by centrifugation until the supernatant was colourless and transparent. The resulting PDA-HNTs were lyophilized on a Freezone freeze dry system (Labconco corporation). The typical mass of product was 22.3 mg.

PDA-HNTs were surface coated with (PEG-$NH_2$) via Michael Addition. In a typical synthesis 20 mg of PDA-HNT was ultrasonically dispersed (100 W, 10 s) in 20 ml of 10 mM Tris-HCl buffer (pH 8.5). Subsequently, 20 mg of mPEG-$NH_2$ was added to the dispersion under constant stirring. After 24 hours, PEG-PDA-HNTs were obtained by centrifugation and washing via DI $H_2O$ repeatedly until the supernatant was colourless and transparent. The typical mass of product was 19.98 mg.

To remove the halloysite template, 200 mg PDA-HNTs or PEG-PDA-HNTs were added to 1.52 ml HCl with mild stirring, then 0.76 ml 50% HF was added dropwise. After 24 hours stirring at room temperature the product was centrifuged and washed by DI H2O repeatedly, typically six cycles, until the supernatant pH was over 5. The collected precipitate was lyophilized prior to subsequent use. The typical mass of product was 40.09 mg.

**Synthesis of polydopamine nanospheres (PDA-NS) and polyethylene glycol coated PDA nanospheres (PEG-PDA-NS).** PDA-NS were synthesized via the method reported by Liu et. al.[2] In a typical synthesis two ml, ammonia aqueous solution ($NH_4OH$, 28-30%) was added dropwise to an ethanol : water solution (40 ml ethanol : 90 ml DI $H_2O$) under constant stirring at 30 ℃. Subsequently, 0.5 g DA, dissolved in 10 ml DI $H_2O$ was added. After 24 h, the product (PDA-NS) was obtained via centrifugation and washing by DI $H_2O$ repeatedly until the supernatant was colourless and transparent. The product was lyophilized prior to further investigation. The typical mass of product was 95.04 mg.

PDA-NS were surface coated with PEG-NH2 via Michael Addition. Using similar condition as were used to produce PEG-PDA-HNTs. In a typical synthesis between 20 mg of PDA-NS was ultrasonically dispersed (100 W, 10 s) in 30 ml of 10 mM Tris-HCl buffer (pH 8.5). Subsequently, 40 mg of mPEG-NH2 dissolved in 4 ml DI water was added to the dispersion under constant stirring. After 24 hours, PEG-PDA-NS were obtained by centrifugation and washing via DI H2O repeatedly until the supernatant was colourless and transparent. The typical mass of product was 30 mg.

#### Characterization

**Drug loading of Doxorubicin on PEG-PDA-NTs and PEG-PDA-NS.** Loading was performed by adsorption of doxorubicin by PEG-PDA-NTs or PEG-PDA-NS from solutions (1.5, 1, 0.5, 0.25, 0.1 mg/ml) of doxorubicin in phosphate buffer (PBS; 10 mM, pH 8). PEG-PDA-NT or PEG-PDA-NP was dispersed into the solutions at a concentration of 0.5 mg/ml under magnetic stirring at room temperature. After 24 hours, the doxorubicin loaded PEG-PDA-NT or PEG-PDA-NS (PEG-PDA-NT/Dox or PEG-PDA-NS/Dox) was collected via centrifugation and washed via fresh PBS (10 mM, pH 7.4) three times to remove extra unloaded Dox.

**Photothermal effect of PEG-PDA-NT and PEG-PDA-NS.** The temperature rise of dispersions upon irradiation was used to evaluate photothermal conversion efficiency. PEG-PDA-NT or PEG-PDA-NS were placed in 1 ml DI $H_2O$ in a 10 mm x 10 mm quartz cuvette. The temperature of the solution was monitored until the sample was at thermal equilibrium with the room. The cuvette was then irradiated with 808 nm wavelength light using a fibre light guide. Intensity at the cuvette surface was ~1 W/$cm^2$. A thermocouple was inserted into the medium and out of the laser path. The temperature of the dispersion was recorded every 10 seconds.

**Stimuli-responsive drug release.** The effect of irradiation and medium pH changes were evaluated by monitoring the amount of doxorubicin released into the dispersion medium over time. In a typical experiment, to examine the effect of pH, 2 mg doxorubicin loaded nanoparticles were added to 30 ml PBS (10 mM, pH 7.4 or pH 5) with mild stirring at room temperature. Periodically, 3 ml release medium was collected and centrifuged (21,964 g for 1 min). The concentration of doxorubicin in the supernatant was determined by UV-Vis absorption at 480 nm, and used to determine the total amount of doxorubicin released from the nanoparticles. The precipitate was dispersed in 3 ml of fresh PBS and returned to the sample. The influence of NIR on drug release was investigated using a similar methodology. In a typical experiment, 0.2 mg of doxorubicin loaded nanoparticles was added to 3 ml PBS (10 mM, pH 7.4 or 5) with mild stirring at room temperature, and placed in a quartz cuvette. NIR irradiation (808 nm, ~1 W/$cm^2$ at sample surface) was applied to the top of the sample for 10 minutes every 110 min. Just prior to and immediately after each irradiation cycle, a 0.2 ml sample was collected and centrifuged. After the doxorubicin concentration in the supernatant was determined by UV-Vis, the precipitate was dispersed in the same supernatant and returned to the cuvette.

## Conclusions

Hollow bilayer polyethylene glycol polydopamine nanotubes were prepared via the use of halloysite as a sacrificial template. The abundant catechol and amino groups on polydopamine enable surface coating of halloysite under mild conditions, and enable grafting of polyethylene glycol on the outer surface by a Michael Addition mechanism. The halloysite core prevents similar grafting on the inner surface of the polydopamine layer resulting in a bilayer nanotube after the template is removed. The prepared tubes exhibited excellent photothermal behavior. Compared to polyethylene glycol coated polydopamine spheres, the nanotubes displayed significantly higher loading

capacity of a model cancer therapeutic, doxorubicin. The tubular shape and size range of the nanotubes suggest they would exhibit good circulation lifetime and high specific uptake by tumor cells. It was demonstrated that release of doxorubicin could be controlled by media pH and NIR irradiation. The combination of excellent photothermal efficiency, pH and NIR activated release, with the potential for shape dependent enhanced circulatory lifetime and preferential tumor uptake make these nanotubes a promising drug delivery platform for combined chemo-photothermal therapy. The facile approach to PDA nanotube production should stimulate further research on the utility of anisotropic PDA nanoparticles in cancer therapy and other biomedical applications. The work reported here enables studies on the effect of anisotropy on the biocompatibility and toxicity of PDA and provides key in vitro data to motivate in vivo evaluations of PDA nanotubes.

## Conflicts of interest

There are no conflicts to declare

## Acknowledgements

The authors gratefully acknowledge funding from Auburn University Intramural Grants Program, the Auburn University Department of Chemistry for support for FTIR analysis, and Harrison School of Pharmacy Research Instrumentation Facility for assistance with transmission electron microscopy.

## Notes and references

1. H. Lee, S. M. Dellatore, W. M. Miller and P. B. Messersmith, *Science*, 2007, **318**, 426-430.
2. Y. Liu, K. Ai, J. Liu, M. Deng, Y. He and L. Lu, *Advanced Materials*, 2013, **25**, 1353-1359.
3. M. Wu, Q. Wang, D. Zhang, N. Liao, L. Wu, A. Huang and X. Liu, *Colloids and Surfaces B: Biointerfaces*, 2016, **141**, 467-475.
4. F. Liu, X. He, Z. Lei, L. Liu, J. Zhang, H. You, H. Zhang and Z. Wang, *Advanced Healthcare Materials*, 2015, **4**, 559-568.
5. M. Martín, P. Salazar, R. Villalonga, S. Campuzano, J. M. Pingarrón and J. L. González-Mora, *Journal of Materials Chemistry B*, 2014, **2**, 739-746.
6. D. Wang, C. Chen, X. Ke, N. Kang, Y. Shen, Y. Liu, X. Zhou, H. Wang, C. Chen and L. Ren, *ACS Applied Materials & Interfaces*, 2015, **7**, 3030-3040.
7. J. Li, W. Wang, L. Zhao, L. Rong, S. Lan, H. Sun, H. Zhang and B. Yang, *ACS Applied Materials & Interfaces*, 2015, **7**, 11613-11623.
8. S. Wang, X. Zhao, S. Wang, J. Qian and S. He, *ACS Applied Materials & Interfaces*, 2016, **8**, 24368-24384.
9. R. Liu, Y. Guo, G. Odusote, F. Qu and R. D. Priestley, *ACS applied materials & interfaces*, 2013, **5**, 9167-9171.
10. T. Zeng, X.-l. Zhang, H.-y. Niu, Y.-r. Ma, W.-h. Li and Y.-q. Cai, *Applied Catalysis B: Environmental*, 2013, **134-135**, 26-33.
11. L. Q. Xu, W. J. Yang, K.-G. Neoh, E.-T. Kang and G. D. Fu, *Macromolecules*, 2010, **43**, 8336-8339.
12. C. Wang, D. Wang, T. Dai, P. Xu, P. Wu, Y. Zou, P. Yang, J. Hu, Y. Li and Y. Cheng, *Advanced Functional Materials*, 2018, **28**, 1802127.
13. Y. Liu, K. Ai and L. Lu, *Chemical reviews*, 2014, **114**, 5057-5115.
14. J. Borovanský and M. Elleder, *Pigment Cell Research*, 2003, **16**, 280-286.
15. P. Kayatz, G. Thumann, T. T. Luther, J. F. Jordan, K. U. Bartz–Schmidt, P. J. Esser and U. Schraermeyer, *Investigative Ophthalmology & Visual Science*, 2001, **42**, 241-246.
16. N. Ohtaki and M. Seiji, *Journal of Investigative Dermatology*, 1971, **57**, 1-5.
17. L. Mosca, C. De Marco, M. Fontana and M. A. Rosei, *Archives of Biochemistry and Biophysics*, 1999, **371**, 63-69.
18. U. Schraermeyer and M. Dohms, *Pigment Cell Research*, 1996, **9**, 248-254.
19. N. F. Della Vecchia, R. Avolio, M. Alfè, M. E. Errico, A. Napolitano and M. d'Ischia, *Advanced Functional Materials*, 2013, **23**, 1331-1340.
20. L. P. Korzhova, E. V. Frolova, I. Romakov and N. A. Kuznetsova, *Biokhimiia*, 1989, **54**, 992-998.
21. C. J. Bettinger, J. P. Bruggeman, A. Misra, J. T. Borenstein and R. Langer, *Biomaterials*, 2009, **30**, 3050-3057.
22. Q. Liu, B. Yu, W. Ye and F. Zhou, *Macromolecular Bioscience*, 2011, **11**, 1227-1234.
23. X. Zhong, K. Yang, Z. Dong, X. Yi, Y. Wang, C. Ge, Y. Zhao and Z. Liu, *Advanced Functional Materials*, 2015, **25**, 7327-7336.
24. W. Cheng, C. Liang, L. Xu, G. Liu, N. Gao, W. Tao, L. Luo, Y. Zuo, X. Wang and X. Zhang, *Small*, 2017, **13**, 1700623.
25. D. Hauser, M. Estermann, A. Milosevic, L. Steinmetz, D. Vanhecke, D. Septiadi, B. Drasler, A. Petri-Fink, V. Ball and B. Rothen-Rutishauser, *Nanomaterials*, 2018, **8**, 1065.
26. R. Zheng, S. Wang, Y. Tian, X. Jiang, D. Fu, S. Shen and W. Yang, *ACS applied materials & interfaces*, 2015, **7**, 15876-15884.
27. M. Wu, D. Zhang, Y. Zeng, L. Wu, X. Liu and J. Liu, *Nanotechnology*, 2015, **26**, 115102.
28. K. C. Black, J. Yi, J. G. Rivera, D. C. Zelasko-Leon and P. B. Messersmith, *Nanomedicine*, 2013, **8**, 17-28.
29. X. Wang, J. Zhang, Y. Wang, C. Wang, J. Xiao, Q. Zhang and Y. Cheng, *Biomaterials*, 2016, **81**, 114-124.
30. S. Wang, J. Lin, Z. Wang, Z. Zhou, R. Bai, N. Lu, Y. Liu, X. Fu, O. Jacobson and W. Fan, *Advanced Materials*, 2017, **29**, 1701013.
31. Z. Zhou, Y. Yan, K. Hu, Y. Zou, Y. Li, R. Ma, Q. Zhang and Y. Cheng, *Biomaterials*, 2017, **141**, 116-124.
32. Y. Gao, X. Wu, L. Zhou, Y. Su and C. M. Dong, *Macromolecular Rapid Communications*, 2015, **36**, 916-922.
33. X. Wang, C. Wang, X. Wang, Y. Wang, Q. Zhang and Y. Cheng, *Chemistry of Materials*, 2017, **29**, 1370-1376.
34. Y. Wang, Q. Huang, X. He, H. Chen, Y. Zou, Y. Li, K. Lin, X. Cai, J. Xiao and Q. Zhang, *Biomaterials*, 2018, **183**, 10-19.
35. S. H. Kim, I. In and S. Y. Park, *Biomacromolecules*, 2017, **18**, 1825-1835.
36. L. Wang, Y. Yu, Q. Xiang, J. Xu, Z. Cheng and J. Xu, *Sensors and Actuators B: Chemical*, 2018, **255**, 2704-2712.
37. W. Ding, S. A. Chechetka, M. Masuda, T. Shimizu, M. Aoyagi, H. Minamikawa and E. Miyako, *Chemistry–A European Journal*, 2016, **22**, 4345-4350.
38. B. Yu, D. A. Wang, Q. Ye, F. Zhou and W. Liu, *Chemical communications*, 2009, 6789-6791.
39. S. E. McNeil, *Wiley Interdisciplinary Reviews: Nanomedicine and Nanobiotechnology*, 2009, **1**, 264-271.

40. H. Kobayashi, S. Kawamoto, S.-K. Jo, H. L. Bryant, M. W. Brechbiel and R. A. Star, *Bioconjugate Chemistry*, 2003, **14**, 388-394.
41. N. Malik, R. Wiwattanapatapee, R. Klopsch, K. Lorenz, H. Frey, J. W. Weener, E. W. Meijer, W. Paulus and R. Duncan, *Journal of Controlled Release*, 2000, **65**, 133-148.
42. S. S. Nigavekar, L. Y. Sung, M. Llanes, A. El-Jawahri, T. S. Lawrence, C. W. Becker, L. Balogh and M. K. Khan, *Pharmaceutical Research*, 2004, **21**, 476-483.
43. J. A. Champion and S. Mitragotri, *Pharmaceutical Research*, 2009, **26**, 244-249.
44. J. A. Champion and S. Mitragotri, *Proceedings of the National Academy of Sciences*, 2006, **103**, 4930-4934.
45. J. A. Champion, Y. K. Katare and S. Mitragotri, *Journal of controlled release*, 2007, **121**, 3-9.
46. Y. Geng, P. Dalhaimer, S. Cai, R. Tsai, M. Tewari, T. Minko and D. E. Discher, *Nature Nanotechnology*, 2007, **2**, 249.
47. A. Malugin and H. Ghandehari, *Journal of Applied Toxicology: An International Journal*, 2010, **30**, 212-217.
48. Z. Zhou, X. Ma, E. Jin, J. Tang, M. Sui, Y. Shen, E. A. Van Kirk, W. J. Murdoch and M. Radosz, *Biomaterials*, 2013, **34**, 5722-5735.
49. M. Janát-Amsbury, A. Ray, C. Peterson and H. Ghandehari, *European Journal of Pharmaceutics and Biopharmaceutics*, 2011, **77**, 417-423.
50. K. C. L. Black, Y. Wang, H. P. Luehmann, X. Cai, W. Xing, B. Pang, Y. Zhao, C. S. Cutler, L. V. Wang, Y. Liu and Y. Xia, *ACS Nano*, 2014, **8**, 4385-4394.
51. V. P. Chauhan, Z. Popović, O. Chen, J. Cui, D. Fukumura, M. G. Bawendi and R. K. Jain, *Angewandte Chemie International Edition*, 2011, **50**, 11417-11420.
52. O. Shimoni, Y. Yan, Y. Wang and F. Caruso, *ACS Nano*, 2013, **7**, 522-530.
53. K. Zhang, H. Fang, Z. Chen, J.-S. A. Taylor and K. L. Wooley, *Bioconjugate Chemistry*, 2008, **19**, 1880-1887.
54. L. Florez, C. Herrmann, J. M. Cramer, C. P. Hauser, K. Koynov, K. Landfester, D. Crespy and V. Mailänder, *Small*, 2012, **8**, 2222-2230.
55. K. Niikura, T. Matsunaga, T. Suzuki, S. Kobayashi, H. Yamaguchi, Y. Orba, A. Kawaguchi, H. Hasegawa, K. Kajino, T. Ninomiya, K. Ijiro and H. Sawa, *ACS Nano*, 2013, **7**, 3926-3938.
56. S. Barua, J.-W. Yoo, P. Kolhar, A. Wakankar, Y. R. Gokarn and S. Mitragotri, *Proceedings of the National Academy of Sciences*, 2013, **110**, 3270.
57. N. Doshi and S. Mitragotri, *PLOS One*, 2010, **5**, e10051.
58. X. Zhao, S. Ng, B. C. Heng, J. Guo, L. Ma, T. T. Y. Tan, K. W. Ng and S. C. J. Loo, *Archives of Toxicology*, 2013, **87**, 1037-1052.
59. A. L. van de Ven, P. Kim, O. H. Haley, J. R. Fakhoury, G. Adriani, J. Schmulen, P. Moloney, F. Hussain, M. Ferrari, X. Liu, S.-H. Yun and P. Decuzzi, *Journal of Controlled Release*, 2012, **158**, 148-155.
60. X. Huang, L. Li, T. Liu, N. Hao, H. Liu, D. Chen and F. Tang, *ACS Nano*, 2011, **5**, 5390-5399.
61. R. Riahi, A. Tamayol, S. A. M. Shaegh, A. M. Ghaemmaghami, M. R. Dokmeci and A. Khademhosseini, *Current Opinion in Chemical Engineering*, 2015, **7**, 101-112.
62. S. Xu, Z. Nie, M. Seo, P. Lewis, E. Kumacheva, H. A. Stone, P. Garstecki, D. B. Weibel, I. Gitlin and G. M. Whitesides, *Angewandte Chemie*, 2005, **117**, 734-738.
63. D. Dendukuri, K. Tsoi, T. A. Hatton and P. S. Doyle, *Langmuir*, 2005, **21**, 2113-2116.
64. D. Dendukuri, D. C. Pregibon, J. Collins, T. A. Hatton and P. S. Doyle, *Nature Materials*, 2006, **5**, 365.
65. D. A. Canelas, K. P. Herlihy and J. M. DeSimone, *Wiley Interdisciplinary Reviews: Nanomedicine and Nanobiotechnology*, 2009, **1**, 391-404.
66. N. Doshi and S. Mitragotri, *Journal of The Royal Society Interface*, 2010, **7**, S403-S410.
67. Y. Geng, P. Dalhaimer, S. Cai, R. Tsai, M. Tewari, T. Minko and D. E. Discher, *Nature Nanotechnology*, 2007, **2**, 249.
68. S. E. Lohse and C. J. Murphy, *Chemistry of Materials*, 2013, **25**, 1250-1261.
69. L. Scarabelli, M. Grzelczak and L. M. Liz-Marzán, *Chemistry of Materials*, 2013, **25**, 4232-4238.
70. D. Li, Z. Tang, Y. Gao, H. Sun and S. Zhou, *Advanced Functional Materials*, 2016, **26**, 66-79.
71. C. J. Ward, R. Tronndorf, A. S. Eustes, M. L. Auad and E. W. Davis, *Journal of Nanomaterials*, 2014, **2014**, 47.
72. G. L. Li, J. Hu, H. Wang, C. Pilz-Allen, J. Wang, T. Qi, H. Möhwald and D. G. Shchukin, *Polymer*, 2017, **109**, 332-338.
73. T. Sun, Y. S. Zhang, B. Pang, D. C. Hyun, M. Yang and Y. Xia, *Angewandte Chemie International Edition*, 2014, **53**, 12320-12364.
74. J. Yu, X. Bai, J. Suh, S. B. Lee and S. J. Son, *Journal of the American Chemical Society*, 2009, **131**, 15574-15575.
75. B. Newland, C. Taplan, D. Pette, J. Friedrichs, M. Steinhart, W. Wang, B. Voit, F. Seib and C. Werner, *Nanoscale*, 2018, **10**, 8413-8421.
76. G. Chen, R. Chen, C. Zou, D. Yang and Z.-S. Chen, *Journal of Materials Chemistry B*, 2014, **2**, 1327-1334.
77. W. O. Yah, H. Xu, H. Soejima, W. Ma, Y. Lvov and A. Takahara, *Journal of the American Chemical Society*, 2012, **134**, 12134-12137.
78. M. R. Abidian, D.-H. Kim and D. C. Martin, *Advanced Materials*, 2006, **18**, 405-409.
79. A. Huczko, *Applied Physics A*, 2000, **70**, 365-376.
80. P.-C. Ma, N. A. Siddiqui, G. Marom and J.-K. Kim, *Composites Part A: Applied Science and Manufacturing*, 2010, **41**, 1345-1367.
81. S. Daniel, T. P. Rao, K. S. Rao, S. U. Rani, G. R. K. Naidu, H.-Y. Lee and T. Kawai, *Sensors and Actuators B: Chemical*, 2007, **122**, 672-682.
82. N. G. Sahoo, S. Rana, J. W. Cho, L. Li and S. H. Chan, *Progress in Polymer Science*, 2010, **35**, 837-867.
83. Y. Wang, X. Su, P. Ding, S. Lu and H. Yu, *Langmuir*, 2013, **29**, 11575-11581.
84. J. Xue, W. Zheng, L. Wang and Z. Jin, *ACS Biomaterials Science & Engineering*, 2016, **2**, 489-493.
85. D. Yan, P. Xu, Q. Xiang, H. Mou, J. Xu, W. Wen, X. Li and Y. Zhang, *Journal of Materials Chemistry A*, 2016, **4**, 3487-3493.
86. D. Fan, X. Zhu, Q. Zhai, E. Wang and S. Dong, *Analytical chemistry*, 2016, **88**, 9158-9165.
87. P. Yuan, P. D. Southon, Z. Liu, M. E. R. Green, J. M. Hook, S. J. Antill and C. J. Kepert, *The Journal of Physical Chemistry C*, 2008, **112**, 15742-15751.
88. M. Liu, Z. Jia, D. Jia and C. Zhou, *Progress in Polymer Science*, 2014, **39**, 1498-1525.
89. V. A. Vinokurov, A. V. Stavitskaya, Y. A. Chudakov, E. V. Ivanov, L. K. Shrestha, K. Ariga, Y. A. Darrat and Y. M. Lvov, *Science and Technology of Advanced Materials*, 2017, **18**, 147-151.
90. B. Singh, *Clays and Clay Minerals*, 1996, **44**, 191-196.
91. Y. M. Lvov, D. G. Shchukin, H. Möhwald and R. R. Price, *ACS Nano*, 2008, **2**, 814-820.
92. C. J. Ward, S. Song and E. W. Davis, *Journal of Nanoscience and Nanotechnology*, 2010, **10**, 6641-6649.

93. C. J. Ward, M. DeWitt and E. W. Davis, *Nanomaterials for Biomedicine*, 2012, **10**, 209-238.
94. E. Abdullayev and Y. Lvov, *Journal of Materials Chemistry B*, 2013, **1**, 2894-2903.
95. R. K. Jain and T. Stylianopoulos, *Nature Reviews Clinical Oncology*, 2010, **7**, 653.
96. A. Xie, J. Dai, X. Chen, T. Zou, J. He, Z. Chang, C. Li and Y. Yan, *RSC Advances*, 2016, **6**, 51014-51023.
97. Y. Liu, H. Nan, Q. Cai and H. Li, *Journal of Applied Polymer Science*, 2012, **125**, E638-E643.
98. N. F. Della Vecchia, A. Luchini, A. Napolitano, G. D'Errico, G. Vitiello, N. Szekely, M. d'Ischia and L. Paduano, *Langmuir*, 2014, **30**, 9811-9818.
99. Y. Li, C. Jiang, D. Zhang, Y. Wang, X. Ren, K. Ai, X. Chen and L. Lu, *Acta Biomaterialia*, 2017, **47**, 124-134.
100. X. Liu, J. Cao, H. Li, J. Li, Q. Jin, K. Ren and J. Ji, *ACS Nano*, 2013, **7**, 9384-9395.
101. R. Luo, L. Tang, J. Wang, Y. Zhao, Q. Tu, Y. Weng, R. Shen and N. Huang, *Colloids and Surfaces B: Biointerfaces*, 2013, **106**, 66-73.
102. Y. Chen, Y. Zhang, J. Liu, H. Zhang and K. Wang, *Chemical Engineering Journal*, 2012, **210**, 298-308.
103. H. Luo, C. Gu, W. Zheng, F. Dai, X. Wang and Z. Zheng, *RSC Advances*, 2015, **5**, 13470-13477.
104. G. Razzano, V. Rizzo and A. Vigevani, *Farmaco*, 1990, **45**, 215-222.
105. Z. Fülöp, R. Gref and T. Loftsson, *International Journal of Pharmaceutics*, 2013, **454**, 559-561.
106. W. Chen, J. Ouyang, H. Liu, M. Chen, K. Zeng, J. Sheng, Z. Liu, Y. Han, L. Wang, J. Li, L. Deng, Y.-N. Liu and S. Guo, *Advanced Materials*, 2017, **29**, 1603864.
107. X. Huang, S. Neretina and M. A. El-Sayed, *Advanced materials*, 2009, **21**, 4880-4910.
108. E. C. Dreaden, S. W. Morton, K. E. Shopsowitz, J.-H. Choi, Z. J. Deng, N.-J. Cho and P. T. Hammond, *ACS Nano*, 2014, **8**, 8374-8382.
109. E. S. Lee, K. T. Oh, D. Kim, Y. S. Youn and Y. H. Bae, *Journal of Controlled Release*, 2007, **123**, 19-26.
110. Q. Liu, X. Chen, J. Jia, W. Zhang, T. Yang, L. Wang and G. Ma, *ACS Nano*, 2015, **9**, 4925-4938.

**Table of Contents Entry and Statement.**

Entry:

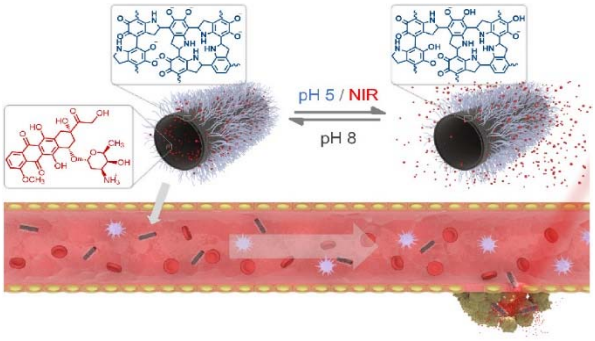


Statement:

Polydopamine nanoparticles with higher drug loading capacity and enhanced photothermal behavior.